Title: An Extra-Large Pore Zeolite Enabled by 1D-to-3D Topotactic Condensation

Authors: Jian Li[1,2,3,13,14,15*], Zihao Rei Gao[2,4,14], Qing-Fang Lin[5,14], Chenxu Liu[6], Fangxin Gao[5], Cong Lin[2,3,7], Siyao Zhang[5], Hua Deng[8], Alvaro Mayoral[9,10], Wei Fan[11], Song Luo[11], Xiaobo Chen[12], Miguel A. Camblor[4,15*], Fei-Jian Chen[5,6,15*] & Jihong Yu[6,15*]

Affiliations:

1 Berzelii Center EXSELENT on Porous Materials, Department of Materials and Environmental Chemistry, Stockholm University, Stockholm, 10691, Sweden.

2 Anhui ZEO New Material Technology Co., 778 Dongliu Road, Hefei, 230071, China.

3 College of Chemistry and Molecular Engineering, Peking University, Beijing, China.

4 Instituto de Ciencia de Materiales de Madrid, Consejo Superior de Investigaciones Científicas (ICMM-CSIC), c/Sor Juana Inés de la Cruz 3, Madrid 28049, Spain.

5 Department of Chemistry, Bengbu Medical College, Bengbu, 233030, China.

6 State Key Laboratory of Inorganic Synthesis and Preparative Chemistry, College of Chemistry; International Center of Future Science, Jilin University, Changchun, China.

7 Department of Mechanical Engineering, The Hong Kong Polytechnic University, Kowloon, Hong Kong, China.

8 Center for Excellence in Regional Atmospheric Environment, Key Laboratory of Urban Pollutant Conversion, Institute of Urban Environment, Chinese Academy of Sciences, Xiamen, 361021, China

9 Instituto de Nanociencia y Materiales de Aragón (INMA), CSIC-Universidad de Zaragoza, Zaragoza 50009, Spain

10 Laboratorio de Microscopias Avanzadas (LMA-Universidad de Zaragoza), 50018, Zaragoza, Spain

11 Department of Chemical Engineering, University of Massachusetts, Amherst, MA 01003, USA.

12 State Key Laboratory of Heavy Oil Processing, China University of Petroleum, Qingdao 266580, China.

13 Present address: Department of Fibre and Polymer Technology, School of Engineering Sciences in Chemistry, Biotechnology and Health, KTH Royal Institute of Technology, Tekninkringen 56-58, Stockholm, SE-100 44, Sweden.

14 These authors contributed equally: Jian Li, Zihao Rei Gao, Qing-Fang Lin

15 These authors jointly supervised this work: Jian Li, Miguel A. Camblor, Fei-Jian Chen, Jihong Yu. e-mail: jxpxlijian@pku.edu.cn (J.L.); macamblor@icmm.csic.es (M.A.C.); cfj-cumt@163.com (F.-J.C.); jihong@jlu.edu.cn (J.Y.)

Bold first paragraph:

Zeolites are microporous silicates that find an ample variety of applications as catalysts[1,2], adsorbents[3], and cation exchangers[4]. Natural and synthetic zeolites possess a fully connected three-dimensional network of corner-sharing SiO_4 tetrahedra (*i.e.* they are *tectosilicates* or *framework silicates*[5], with Si occasionally substituted by other atoms). Stable silica-based zeolites with increased porosity are of interest to allow processing of large molecules, but challenge our synthetic ability[6]. Here we report a novel zeolite, ZEO-3, with a multidimensional, interconnected system of extra-large pores open through windows made by 16 and 14 SiO_4 tetrahedra, which, with a specific surface area of over 1000 m^2/g and an extraordinary performance for Volatile Organic Compounds abatement, is the less dense polymorph of silica known so far. This zeolite, however, is not directly synthesized as a tectosilicate but is the first three-dimensional zeolite that is obtained by topotactic condensation from a one-dimensional chain silicate (*inosilicate,* ZEO-2), a process that bears a 17% contraction of the structure but that does not alter the topology of the chain silicate (hence the term "topotactic"). This discovery challenges concepts deeply-rooted into zeolite science, and opens up the possibility of chain silicates as precursors for the crystallization of zeolites.

Main text:

Generally, zeolites are synthesized directly as tectosilicates. However, some zeolites are obtained in the form of two-dimensional precursors (*phyllosilicates* or *layered silicates*)[5] that only become fully connected tectosilicate zeolites by condensation of their layers through a calcination procedure that do not alter the layer topology[7,8], a process that is topotactic because the internal structure of the condensing layers is not altered[9]. The condensing layers can be obtained by direct synthesis or by

dissasembly of certain zeolites as in the so-called ADOR (assembly-disassembly-organization-reassembly) process[10]. However, in around eight decades of extensive and systematic zeolite synthesis studies[11], there has been no example of a three-dimensional (3D) zeolite obtained by condensation from a one-dimensional (1D) precursor, either directly synthesized or obtained by disassembly of another zeolite. We report here the first case of such a 1D-to-3D topotactic condensation from ZEO-2, a complex "zeolitic" chain silicate, into ZEO-3, a fully connected three-dimensional extra-large pore zeolite (ZEO-*n* refers to materials discovered and patented by the Anhui ZEO New Material Technology Co., China). The resulting zeolite ZEO-3 is outstanding for a number of reasons, including its very low density (less than half that of quartz), its multidimensional system of interconnected extra-large pores, and the presence in its structure of double four-member ring units (D4R), *i.e.* small cubes of silica. For pure silica zeolites, this kind of unit is strained and up to now was believed to need a fluoride anion close to its centre to be accessible for crystallization[12] since it has never been seen before in a silica zeolite synthesized without the use of fluoride anions. Only the "reverse ADOR" process, a postsynthetic modification that breaks Ge-containing D4R to then restore them as silica D4R, can also possibly produce these units, although no conclusive proof of the complete silica restoration (^{29}Si MAS NMR, FTIR in the OH stretching region, structural refinement) has been provided so far[13].

The complex chain silica zeolite precursor ZEO-2 can be synthesized using tricyclohexylmethylphosphonium ($C_{19}H_{36}P^+$, tCyMP) from a gel of composition 1 SiO_2 : 0.5 tCyMPOH : 10 H_2O heated at 175 ºC (see Methods). The structure of ZEO-2 was successfully solved *ab initio* by using eight continuous rotation electron diffraction (cRED)[14] datasets and then refined against synchrotron powder X-ray diffraction (SPXRD). The pure silicate ZEO-2 possesses a needle-like morphology (Fig. S1a) and crystallizes in a *C*-centred monoclinic cell with a = 23.5465(7) Å, b = 24.7446(7) Å, c = 14.4024(4) Å, β = 115.1974(9)° (Tab. S1-S2, Fig. S2). ZEO-2 is a 1D chain silicate decorated with silanol/silanolate groups (Fig. 1a) that hold the structure

together through ample hydrogen bonding to adjacent chains (Fig. 1b, 1c), with the tCyMP cations located in the interchain space (Fig. S3). The cations are occluded intact, as demonstrated by ^{13}C and ^{31}P NMR (Fig. S4) and amount to 8.85 OSDA/uc according to C analysis (25.0%). Hydrogen bonds are observed in the ^{1}H magic-angle spinning (MAS) nuclear magnetic resonance (NMR) spectrum as a broad resonance around 15.1 ppm (Fig. S5), indicating a moderate-to-strong hydrogen bond[15] corresponding to the O⋯O distances[16] of around 2.51 Å, in good agreement with the crystallographic distances of 2.47-2.52 Å. Upon calcination to remove the tCyMP, silanol groups in adjacent chains condense into Si-O-Si bridges with H_2O elimination, resulting in the novel pure silica zeolite ZEO-3 (Fig. 1e-1g), which maintains the needle-like morphology (Fig. S1b). The condensation occurs in the 370-390 ^{o}C range (Fig. S6), coincident with the removal of organics (Fig. S7). The structure of ZEO-3 was also solved *ab initio* by 3D ED with five datasets (Tab. S2, S3, Fig. S8), similarly to ZEO-2. The unit cell of ZEO-3 shrinks to a = 21.5046(8) Å, b = 21.2757(8) Å, c = 14.4638(4) Å, β = 108.7196(1)° but maintains the same symmetry as ZEO-2, while the topology of the chain is preserved. In fact, a 17% contraction of the structure occurs along *a*- and *b*- axis, while along *c*-axis only a marginal expansion (0.4%) occurs. To obtain more accurate atomic positions, the structures of ZEO-2 and ZEO-3, including the position of the disordered tCyMP in ZEO-2, were subsequently Rietveld refined against the SPXRD (Extended Data Fig. 1, Fig. S3, Tab. S4-S8). The final refined unit-cell compositions of ZEO-2 and ZEO-3 are $[Si_{80}O_{176}H_{24}]|(C_{19}H_{36}P)_8$ and $Si_{80}O_{160}$, respectively (see Methods for more details).

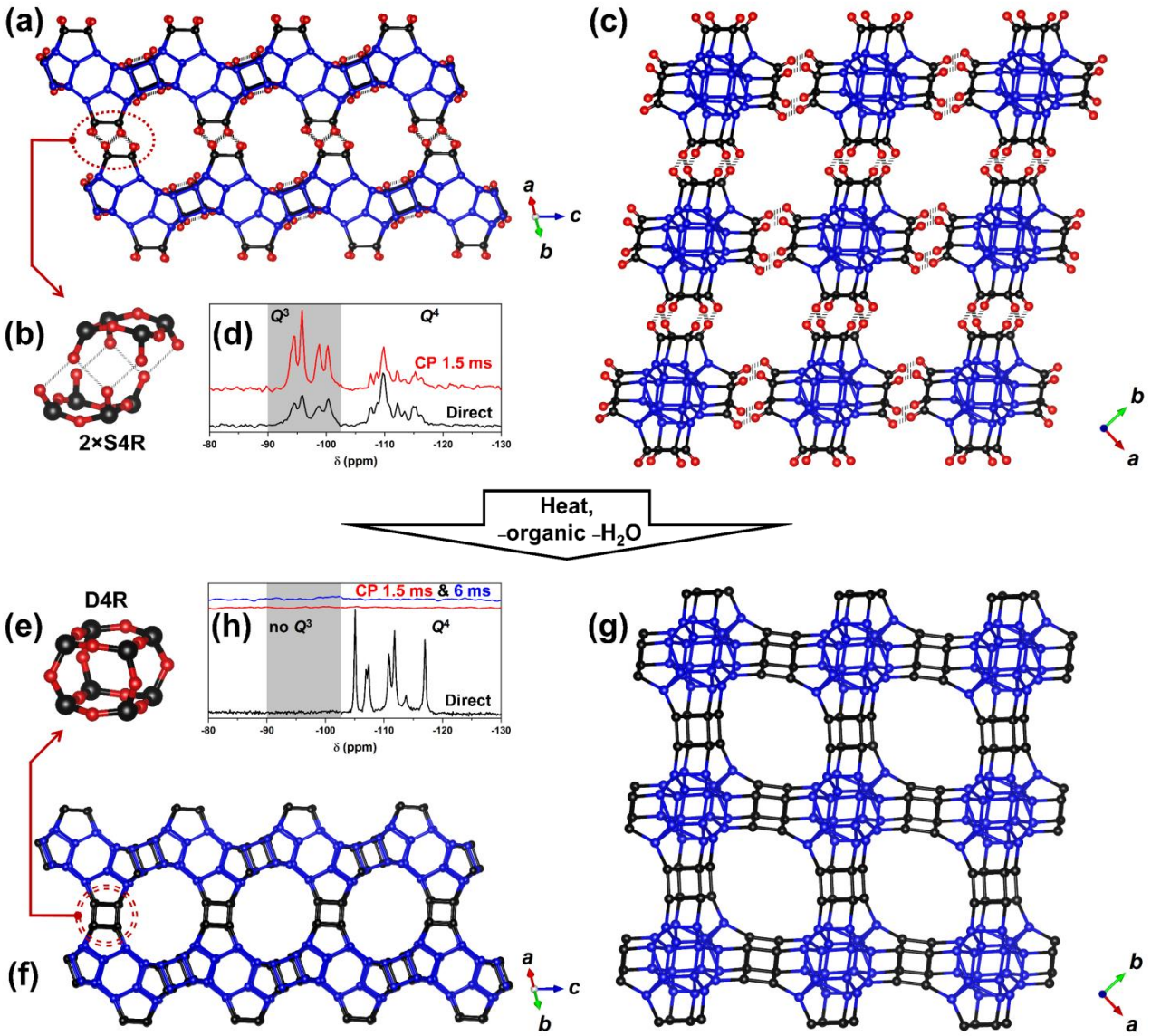

Fig. 1 | The 1D-to-3D topotactic condensation of the chain silicate ZEO-2 (a-d) into the extra-large pore framework zeolite ZEO-3 (e-h). Only O atoms related to the condensation are shown (small red balls) while Si atoms are shown as blue (always Q^4) or black (Q^3 in ZEO-2 converting into Q^4 in ZEO-3). A chain of ZEO-2 (**a**) is hydrogen bonded (**b**) to four adjacent chains (**c**). The ^{29}Si MAS NMR spectrum (**d** bottom) shows resolution of Q^3 and Q^4 silicon sites (4 and 7 sites, respectively). The close proximity of Q^3 sites to H atoms is revealed in the ^{29}Si{^{1}H} cross polarization (CP) MAS NMR spectrum by their relative intensity enhanced by polarization transfer from close protons at short contact time (**d** top, 1.5 ms). Upon calcination, condensation of Q^3 sites through dehydroxilation connects two S4Rs to make a D4R (**e**), through which each chain is bonded to four adjacent chains, resulting in the extra-large pore ZEO-3 with 14MR (**f**) and 16MR (**g**)

channels. The corresponding ^{29}Si MAS NMR spectra (**h** bottom) shows essentially only Q^4 sites with almost no Q^3 defects and hence little intensity enhancement in the ^{29}Si{^{1}H} CP MAS NMR under short (**h** middle, 1.5 ms) or long contact time (**h** top, 6 ms).

The 1D pure silica chains in ZEO-2 are aligned along the [001] direction (Fig. 1a) and surrounded by four identical chains in the *ab* plane (Fig. 1c). At the edge of the ZEO-2 chain, four silanols/silanolates form a single four-member ring (S4R) that faces, slightly displaced, an identical S4R from the next chain, with hydrogen bonding along the [110] and [1-10] directions providing connection between both chains (Fig. 1b). Upon calcination, neighbouring S4Rs in ZEO-2 connect to each other to form a D4R (Fig. 1e) by condensation of the terminal Si-OH groups, yielding the fully-connected framework of ZEO-3 (Fig. 1f, 1g). The condensed solid is a true, non-interrupted, three-dimensional extra-large pore zeolite. The channel system of ZEO-3 is 3D with 16×14×14 membered-ring (MR) channels (Fig. 1f, 1g) and full connectivity between channels (Extended Data Fig. 2). The structural model obtained was fully corroborated by Cs-corrected scanning transmission electron microscopy (STEM). Extended Data Fig. 3 depicts the high-resolution observations of ZEO-2 along [110], where ZEO-2 chains connected by hydrogen bonds leading into the formation of 14 MRs can be observed. Furthermore, a faint signal corresponding to the tCyMP (C and P) is also identified within the 14 MRs (Extended Data Fig. 3a). The fully-connected ZEO-3 on the [110] and [001] projections (Extended data Fig. 3b-c), corresponding to the 14MRs and 16 MRs visualization, respectively, are also presented. In all cases, the simulated STEM image from the structure models has been included in the inset and the schematic models obtained have been overlaid observing a perfect matching between the images and the structural solution proposed. Further electron microscopy data is presented in Fig. S9, including low-magnification images, electron diffraction diffractograms and the fast Fourier transform (FFT) of the images.

As a pure silica zeolite precursor, the resolution of the ^{29}Si MAS NMR spectrum of ZEO-2 is excellent (Fig. 1d), indicating four Q^3 Si sites (-94.2, -95.8, -98.6, and -100.4 ppm) spanning a chemical shift range unprecedented for Q^3 in zeolites (more typically centred at around -102±1 ppm) but well within the general Q^3 range in silicates[17] and seven Q^4 Si sites (from -106.8 to -116.8 ppm), in good agreement with the crystallographic results (4 Q^3 and 5 Q^4 all with the same multiplicity plus 2 Q^4 with half multiplicity, see CIF). ^{29}Si{^{1}H} CP MAS NMR spectroscopy proves the existence of those four Q^3 Si sites in ZEO-2 (Fig. 1d top), while the ^{29}Si MAS NMR spectrum of ZEO-3 shows that in the condensed zeolite essentially all of the Si atoms are Q^4 sites with a negligible amount of Q^3 that could be assigned to the connectivity defects, as proved by the very low intensity enhancement by cross polarization (Fig. 1h).

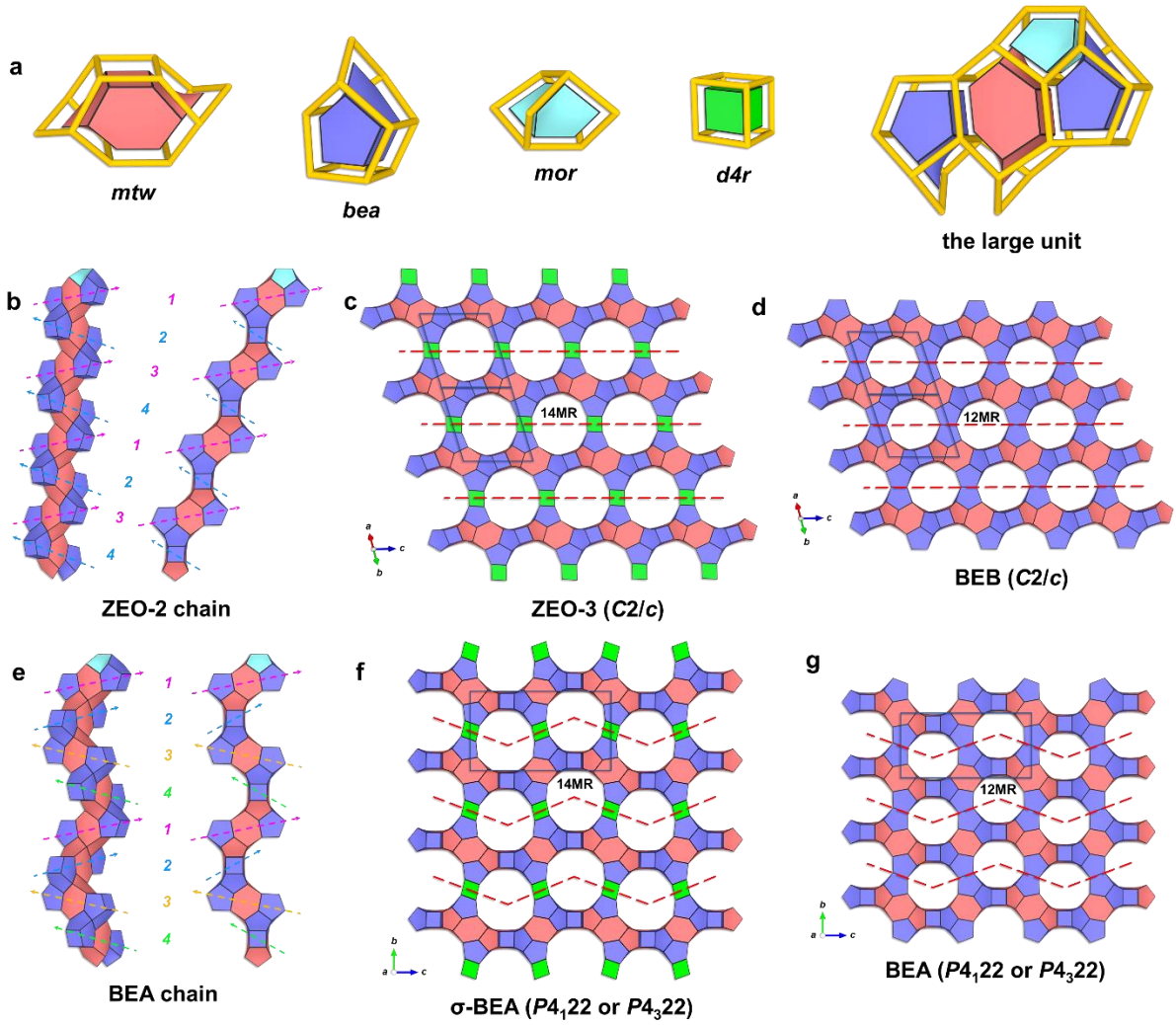

Fig. 2 | Building schemes of ZEO-3 and BEB frameworks from the ZEO-2 chain, and BEA and the hypothetical chiral analogue of ZEO-3 from the BEA chain. (**a**) The individual CBUs and the large unit made from them, (**b**) ZEO-2 chain and (**e**) BEA chain built by attaching successive large units, viewed along two different directions, and tiling structures of (**c**) ZEO-3, (**d**) BEB, (**f**) σ-expanded **BEA**, and (**g**) **BEA**. In (**b**), the dotted arrows indicate four topologically identical large units (units 1, 2, 3, 4) with a +90º, -90º, +90º, -90º, *etc.* rotation in the ZEO-2 chain, where the orientation of units 1 and 3 (and units 4 and 2) is the same. In (**e**), the rotation of successive units is +90º, +90º, +90º, +90º, or -90º, -90º, -90º, -90º, *etc* resulting in the BEA chain, with a chiral nature (space group $P4_122$ or $P4_322$ in **BEA**). In (**c**, **d**, **f**, **g**), the dotted lines separate the neighbouring ZEO-2 or BEA chains; in (**c**) and (**f**), the newly formed D4Rs between neighbouring ZEO-2 or BEA chains are highlighted in green; in (**d**) and (**g**), no D4Rs exist as S4Rs are shared between neighbouring ZEO-2 or BEA chains.

To discuss the details of the topology (Tab. S9-S10), we consider three composite building units (CBUs), *i.e. mtw*, *bea*, and *mor*, which can be used to make a large unit formed by 1 *mtw*, 2 *bea*, and 1 *mor* (Fig. 2a). Successive such units build the ZEO-2 chains with alternative rotations of ± 90^0 (*i.e.* $+90^0$, -90^0, $+90^0$, -90^0, etc.) along the [001] direction (Fig. 2b). This chain is topologically identical to the one found in polymorph B of zeolite Beta (although in that zeolite it is not an isolated chain but is embedded in the 3D framework). For convenience, this polymorph will be called here BEB, although this is not an accepted zeolite code yet (the Structure Commission of the International Zeolite Association assigns three-letter codes to zeolite topologies whose actual existence has been proved)[18]. From ZEO-2 to ZEO-3, the two neighbouring S4Rs mentioned before from two adjacent ZEO-2 chains connect *via* condensation to form a D4R, resulting in the 3D framework of ZEO-3 (Fig. 2c), while in BEB one S4R is shared by two neighbouring chains related by an inversion operation to build the 3D framework (Fig. 2d). The insertion of the additional S4Rs expands the pores from the large 12×12×12 MR pores in BEB into the extra-large 16×14×14 MR

pores in ZEO-3. Considering this description, ZEO-3 is formally a σ transformation of BEB, *i.e.* it results from a systematic insertion of tetrahedral nodes in its structure[19,20]. We point here that, similarly, if the chain were formed by 90^0 rotations always in the same direction of the large unit mentioned above (Fig. 2e), a new chiral 16×14×14MR hypothetical zeolite would result: the σ transformation of polymorph A of zeolite Beta (σ-**BEA**, Fig. 2f). Given that **BEA** and BEB have similar stabilities, we foresee this new chiral extra-large pore zeolite as feasible. We think this chiral structure should be the subject of a search of a proper OSDA by computational means[21]. We also suggest that working in conditions similar to the synthesis of ZEO-3 but in the presence of a chiral OSDA or a chiral auxiliary might be a route worth to explore.

ZEO-3 is the first example of a pure silica zeolite containing D4R synthesized from fluoride-free media, and it is also the first stable, fully connected (alumino)silicate zeolite containing 3D interconnected pores opened only through extra-large windows (*i.e.* windows of more than 12 tetrahedra, >12MR). The crystallographic pore sizes of ZEO-3 are 10.36×8.51 Å and 9.79×8.00 Å for the 16MR and 14MR, respectively (Extended Data Fig. 2). The 3D extra-large pore nature of ZEO-3 translates into a very low framework density (FD) value (12.76 tetrahedral atoms, T-atoms, per 1000 $Å^3$). Compared with the other known stable, low density (alumino)silicate zeolites, including **FAU**, **EMT**, ***BEA**, **BEC**, **ISV**, **IWV**, and the recently reported PST-2, PST-32,[22] and ZEO-1,[6] this value is the lowest and puts ZEO-3 as the crystalline silica polymorph with the most open framework (Tab. S11). The calculated density of ZEO-3 is just 1.27 g/cm^3, *i.e.* less than half that of quartz (2.65 g/cm^3) and actually closer to the density of water. In fact, ZEO-3 breaks the observed tendency between the framework density and the size of the smallest rings in zeolite structure[23]. For an average smallest ring of 4.25, the predicted minimum FD[23] is 13 T-atom per 1000 $Å^3$, above ZEO-3's value. Compared with the real values of non-interrupted zeolites containing 4- and 5-rings, ZEO-3 is well below the lowest calculated FD of **ISV** and **IWV** (15.0; experimental values of 15.4 and 15.7, respectively). Additionally, ZEO-3 is significantly more stable than

expected according to the known energy-density trend, as shown in Fig. S10, while the hypothetical σ-**BEA**, has the expected stability based on the calculation of framework energy after minimization.

The observed N_2 and Ar adsorption/desorption isotherms (type Ia) of ZEO-3 give the very high specific surface area of 989 and 1032 m^2/g (calculated by the Brunauer-Emmett-Teller method, Extended Data Fig. 4-5), respectively, and the non-local density functional theory (NLDFT) method from the Ar adsorption indicates that the mean pore sizes of ZEO-3 are 10.8 and 8.8 Å (Extended Data Fig. 6), matching well with the crystallographic results. The extra-large pores of ZEO-3 allows the diffusion and adsorption of large molecules, like Nile Blue (Extended Data Fig. 7), suggesting potential for the removal of large organic pollutants from waste streams.

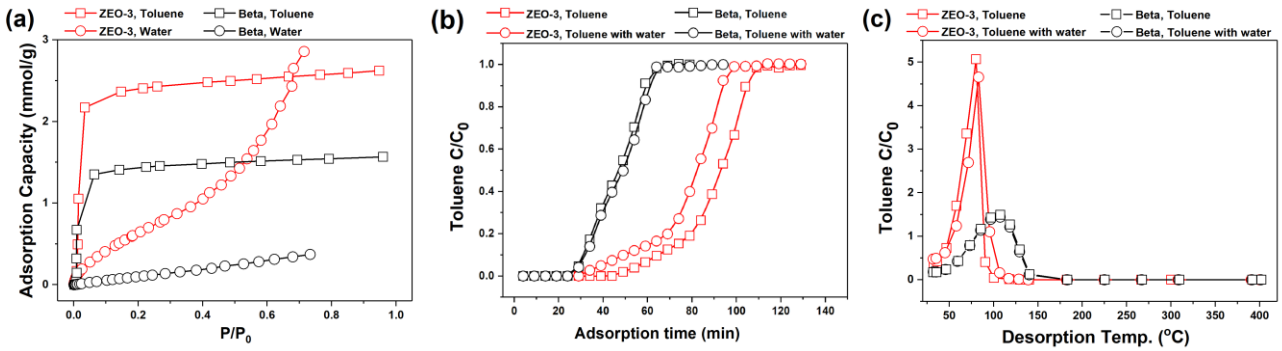

Fig. 3 | Adsorption isotherms (A), breakthrough adsorption (B), and desorption curves (C) on ZEO-3 (red) and Beta (black) zeolite. These data show ZEO-3 outperforms Beta zeolite in terms of high adsorption capacity and good regeneration behaviour.

On the other hand, the vast emissions of volatile organic compounds (VOCs) linked with industrialization severely impact air quality[24]. Adsorption has been considered as one of the most attractive and energy-saving candidates for VOCs abatement. The development of novel sorbents with high adsorption capacity, water vapor resistance and easy regeneration is critical for a

successful adsorption technology[25]. Zeolites are amongst the best adsorbents for VOCs removal due to their unique microporosity, high adsorption capacity, and non-flammable nature[25,26]. ZEO-3 exhibited appealing features for adsorption of VOCs owing to its high surface area and extra-large pores and the hydrophobicity associated to its pure silica composition. Taking typical hydrophobic pure silica Beta as a reference[27,28], equilibrium isotherms, breakthrough curves and desorption curves of toluene are demonstrated in Fig. 3. ZEO-3 outperforms Beta zeolite in terms of high adsorption capacity and good regeneration potential. The outstanding performance under high humidity testifies that ZEO-3 is a promising candidate for VOCs adsorption.

Besides, ZEO-3 shows a high thermal and hydrothermal stability. After calcination in air at 1100 ^{o}C with a one-hour plateau, the crystallinity of ZEO-3 is well maintained, as it is also the case after a steaming treatment at 760 ^{o}C with 10% H_2O vapour for 3 hours. (Extended Data Fig. 8). The Fourier transform infrared (FT-IR) spectrum of ZEO-2 shows a broad and intense resonance centred at around 3194 cm^{-1}, which is characteristic of OH subject to moderate-to-strong hydrogen bonds (Fig. S11). By contrast, the FT-IR spectrum of ZEO-3 after evacuation at 180°C under vacuum shows no signs of hydrogen bonded OH but only a small and relatively sharp band at 3742cm^{-1}, assigned to the "free" (*i.e.* not hydrogen bonded) silanols possibly due to crystallite terminations[29].

The two concepts challenged by ZEO-3 (silica D4R without F and lower FD than predicted) refer actually to observations on materials directly synthesized by hydrothermal crystallization. ZEO-3 shows that materials that may be considered not accessible by direct synthesis can be obtained by post-synthesis transformations, as it has also been observed for zeolites obtained by the assembly-disassembly-organization-reassembly (ADOR)[30] process or the hybrid guest-host pure silica **STW**, which was predicted unfeasible by direct synthesis[31]. This observation allows to foresee new materials developed by 1D-to-3D topotactic condensation. Our work demonstrates complex, zeolitic

silicate chains amenable for 3D condensation may be formed in solution, and hence suggests this type of units should be considered as possible units for the crystal growth of zeolites.

References

1 Zhong, J., Han, J., Wei, Y. & Liu, Z. Catalysts and shape selective catalysis in the methanol-to-olefin (MTO) reaction. *J. Catal*. **396**, 23-31 (2021). doi: 10.1016/j.jcat.2021.01.027.

2 Cui, T.-Y., Rajendran, A., Fan, H.-X., Feng, J. & Li, W.-Y. Review on Hydrodesulfurization over Zeolite-Based Catalysts. *Ind. Eng. Chem. Res*. **60**, 3295-3323 (2021). doi: 10.1021/acs.iecr.0c06234.

3 Wu, Y. & Weckhuysen, B. M. Separation and Purification of Hydrocarbons with Porous Materials. *Angew. Chem. Int. Ed*. **60**, 18930-18949 (2021). doi: 10.1002/anie.202104318; *Angew. Chem*. **133**, 19078-19097 (2021). doi: 10.1002/ange.202104318.

4 Montalvo, S., Huiliñir, C., Borja, R., Sánchez, E. & Herrmann, C. Application of zeolites for biological treatment processes of solid wastes and wastewaters – A review. *Biores. Tech*. **301**, 122808 (2020). doi: 10.1016/j.biortech.2020.122808.

5 Liebau, F. Nomenclature and Structural Formulae of Silicate Anions and Silicates. *Structural Chemistry of Silicates*, Springer-Verlag, Berlin, pp. 72 (1985). doi: 10.1007/978-3-642-50076-3_5.

6 Lin, Q.-F., Gao, Z. R., Lin, C., Zhang, S., Chen, J., Li, Z., Liu, X., Fan, W., Li, J., Chen, X., Camblor, M. A. & Chen, F.-J. A Stable Zeolite Catalyst with Intersecting Three-Dimensional extralarge Plus Large Pores. *Science*, in press. doi: 10.1126/science.abk3258.

7 Schreyeck, L., Caullet, P., Mougenel, J.-C., Guth, J.-L. & Marler, B. A Layered Microporous Aluminosilicate Precursor of FER-type Zeolite. *J. Chem. Soc. Chem. Commun*. 2187-2188 (1995). doi: 10.1039/C39950002187.

8 Millini, R., Perego, G., Parker Jr., W. O., Bellussi, G. & Carluccio, L. Layered structure of ERB-1 microporous borosilicate precursor and its intercalation properties towards polar molecules. *Microporous Mater*. **4**, 221-230 (1995). doi: 10.1016/0927-6513(95)00013-Y.

9 Marler, B., & Gies, H. Hydrous layer silicates as precursors for zeolites obtained through topotactic condensation: a review. *Eur. J. Mineral*. **24**, 405-428 (2012). doi: 10.1127/0935-1221/2012/0024-2187.

10 Eliášová, P., Opanasenko, M., Wheatley, P. S., Shamzhy, M., Mazur, M., Nachtigall, P., Roth, W. J., Morris, R. E. & Čejka, J. The ADOR mechanism for the synthesis of new zeolites. *Chem. Soc. Rev*. **44**, 7177-7206 (2015). doi: 10.1039/c5cs00045a.

11 Cundy, C. S. & Cox, P. A. The Hydrothermal Synthesis of Zeolites: History and Development from the Earliest Days to the Present Time. *Chem. Rev*. **103**, 663-702 (2003). doi: 10.1021/cr020060i.

12 Zicovich-Wilson, C. M., San-Román, M. L., Camblor, M. A., Pascale, F. & Durand-Niconoff, J. S. Structure, Vibrational Analysis, and Insights into Host-Guest Interactions in As-Synthesized Pure Silica ITQ-12 Zeolite by Periodic B3LYP Calculations. *J. Am. Chem. Soc*. **129**, 11512-11523 (2007). doi: 10.1021/ja0730361.

13 Veselý, O., Eliášová, P., Morris, R. E. & Čejka, J. Reverse ADOR: reconstruction of UTL zeolite from layered IPC-1P. *Mater. Adv*. **2**, 3862-3870 (2021). doi: 10.1039/D1MA00212K.

14 Gemmi, M., Mugnaioli, E., Gorelik, T. E., Kolb, U., Palatinus, L., Boullay, P., Hovmöller, S. & Abrahams, J. P. 3D Electron Diffraction: The Nanocrystallography Revolution. *ACS Cent. Sci*. **5**, 1315-1329 (2019). doi: 10.1021/acscentsci.9b00394.

15 Steiner, T. The Hydrogen Bond in the Solid State. *Angew. Chem. Int. Ed*. **41**, 48-76 (2002). doi: 10.1002/1521-3773(20020104)41:1<48::AID-ANIE48>3.0.CO;2-U.

16 Eckert, H., Yesinowski, J. P., Silver, L. A. & Stolper, E. M. Water in Silicate Glasses: Quantitation and Structural Studies by 1H Solid Echo and MAS-NMR Methods. *J. Phys. Chem*. **92**, 2055-2064 (1988). doi: 0022-3654/88/2092-2055S01.50/0.

17 Engelhardt, G. Multinuclear solid-state NMR in silicate and zeolite chemistry. *TrAC Trends Anal. Chem*. **8**, 343-347 (1989). doi: 10.1016/0165-9936(89)87043-8.

18 Baerlocher, C., McCusker, L. B. & Olson D. H. *Atlas of Zeolite Framework Types*, 6th ed. Elsevier, Amsterdam (2007). ISBN: 978-0-444-53064-6.

19 Barrer, R. M. *Hydrothermal Chemistry of Zeolites*, Academic Press, London, pp. 11 (1982).

20 Smith, J. V. Topochemistry of zeolites and related materials. 1. Topology and geometry. *Chem. Rev*. **88**, 149-182 (1988). doi: 0009-2665/88/0788-0149$06.50/0.

21 Schmidt, J. E., Deem, M. W. & Davis, M. E. Synthesis of a Specified, Silica Molecular Sieve by Using Computationally Predicted Organic Structure-Directing Agents. *Angew. Chem. Int. Ed*. **53**, 8372-8374 (2014). doi: 10.1002/anie.201404076; *Angew. Chem*. **126**, 8512-8514 (2014). doi: 10.1002/ange.201404076.

22 Lee, H., Shin, J., Lee, K., Choi, H. J., Mayoral, A., Kang, N. Y. & Hong, S. B. Synthesis of thermally stable SBT and SBS/SBT intergrowth zeolites. *Science*, **373**, 104-107 (2021). doi: 10.1126/science.abi7208.

23 Brunner, G. O. & Meier, W. M. Framework density distribution of zeolite-type tetrahedrals nets. *Nature* **337**, 146-147 (1989). doi: 10.1038/337146a0.

24 Li, M., Zhang, Q., Zheng, B., Tong, D., Lei, Y., Liu, F., Hong, C., Kang, S., Yan, L., Zhang, Y., Bo, Y., Su, H., Cheng, Y., & He, K. Persistent growth of anthropogenic non-methane volatile organic compound (NMVOC) emissions in China during 1990-2017: drivers, speciation and ozone formation po-tential. *Atmos. Chem. Phys*. **19**, 8897-8913 (2019). doi: 10.5194/acp-19-8897-2019.

25 Yang, C., Miao, G., Pi, Y., Xia, Q., Wu, J., Li, Z. & Xiao, J. Abatement of various types of VOCs by adsorption/catalytic oxidation: A review. *Chem. Eng. J*. **370**, 1128-1153 (2019). doi: 10.1016/j.cej.2019.03.232.

26 Veerapandian, S. K. P., De Geyter, N., Giraudon, J.-M., Lamonier, J.-F. & Morent, R. The Use of Zeolites for VOCs Abatement by Combining Non-Thermal Plasma, Adsorption, and/or Catalysis: A Review. *Catalysts* **9**, 98, (2019). doi: 10.3390/catal9010098.

27 Blasco, T., Camblor, M. A., Corma, A., Esteve, P., Guil, J. M., Martínez, A., Perdigón-Melón, J. A. & Valencia S. Direct Synthesis and Characterization of Hydrophobic Aluminum-Free Ti-Beta Zeolite. *J. Phys. Chem. B* **102**, 75-88 (1998). doi: 10.1021/jp973288w.

28 Zhu, Z., Xu, H., Jiang, J., Wu, H. & Wu, P. Hydrophobic Nanosized All-Silica Beta Zeolite: Efficient Synthesis and Adsorption Application. *ACS Appl Mater Interfaces* **9**, 27273-27283 (2017). doi: 10.1021/acsami.7b06173.

29 Dib, E., Costa, I. M., Vayssilov, G. N., Aleksandrov, H. A. & Mintova, S. Complex H-bonded silanol network in zeolites revealed by IR and NMR spectroscopy combined with DFT calculations. *J. Mater. Chem. A*, Advance Article (2021). doi: 10.1039/D1TA06908J.

30 Mazur, M., Wheatley, P. S., Navarro, M., Roth, W. J., Položij, M., Mayoral, A., Eliášová, P., Nachtigall, P., Čejka, J. & Morris, R. E. Synthesis of ‘unfeasible’ zeolites. *Nature Chem*. **8**, 58-62 (2016). doi: 10.1038/nchem.2374.

31 Rojas, A. & Camblor, M. A. A Pure Silica Chiral Polymorph with Helical Pores. *Angew. Chem. Int. Ed*. **51**, 3854-3856 (2012). doi: 10.1002/anie.201108753; *Angew. Chem*. **124**, 3920-3922 (2012). doi: 10.1002/ange.201108753.

Methods

Zeolite syntheses. ZEO-2 was synthesized using the organic structure-directing agent (OSDA) tCyMP$^+$, synthesized following a previously reported protocol[6], from a gel of composition 0.5 OSDAOH : 1 SiO_2 : 10 H_2O at 175 ^oC for 30 days. Specifically, 2.5094 g (12.05 mmol) of TEOS (tetraethylorthosilicate) was mixed and stirred with 33.9454 g (6.002 mmol, c = 0.1768 mmol/g) of OSDAOH overnight for the total hydrolyzation and ethanol evaporation. Once the water content reached the goal (2.1618 g or 120 mmol water in this case), the whole content was transferred into a 30-mL Teflon-inserted autoclave. The autoclave was maintained at 175 ^oC for 30 days without rotation. After crystallization, the solid product was collected, washed with water (30 mL × 2) and acetone (30 mL × 1), dried, and finally identified by PXRD and field-emission scanning electron microscopy (FE-SEM) to get the pure ZEO-2 sample (1.020 g; yield: 21.66 g per 100 g gel).

ZEO-3 was obtained by calcination of ZEO-2 in air at 600 ^oC, with a 3-hour ramp and a 6-hour plateau. Phosphorous residues may be eliminated by washing with water within an autoclave at 100 ^oC for 1 day, or by reduction with H_2 (H_2/N_2, v/v = 10/90) from the as-made ZEO-2 sample at 600 ^oC with a 2-hour ramp and a 6-hour plateau. The thermal stability of the P-free ZEO-3 sample was examined by heating at 800, 900, 1000, and 1100 ^oC (heating rate of 10 ^oC/min and 1-hour plateau at the target temperature). ZEO-3 is also hydrothermally stable (760 ^oC, 10% H_2O, 3 hours). The corresponding PXRD patterns are all shown in Extended Data Fig. 8.

***Ab initio* structure solution by cRED.** The *ab initio* structure solution of ZEO-2 and ZEO-3 were conducted on the needle-like crystals using JEOL JEM-2100 transmission electron microscope (TEM, Cs: 1.0 mm, point resolution: 0.23 nm) at 200 kV. Before the data collection, a droplet of suspension was transferred onto a copper grid. During the data collection, the goniometer was rotated continuously while the selected-area ED patterns were captured from the individual crystal simultaneously by a quad hybrid pixel detector (QTPX-262k, 512×512 pixels with the size of 55 μm, Amsterdam Sci. Ins.) with video mode, using the software *instamatic* script[32]. All the ED patterns were recorded under spot size 3 with an exposure time of 0.5 s. Data processing was

conducted using the software packages XDS [33] and REDp [34]. In order to improve the data completeness, 8 and 5 datasets were collected for ZEO-2 and ZEO-3, respectively. Structure solution was performed using SHELXT [35] with merged and scaled datasets, from which all the framework atoms (11 Si atoms and 22 O atoms in the asymmetric unit of ZEO-2 and 11 Si atoms and 20 O atoms in the asymmetric unit of ZEO-3) were located directly. Then, the framework was refined using Olex 2 [36], with atomic scattering factors for electrons.

Rietveld refinement. In order to obtain more accurate structures and locate the position of OSDA, Rietveld refinement of ZEO-2 and ZEO-3 were performed against SPXRD patterns, which were collected under 100 K at the 11-BM beamline of the Advanced Photon Source at Argonne National Laboratory, USA, with a wavelength of 0.458086 Å. The structure from cRED data was used as the initial model for the Rietveld refinement with the software Topas 6.1 [37]. Before refinement, an optimization of the framework geometry was performed by using the distance-least-squares algorithm. In the initial stages of the refinement, soft restraints were placed on the Si-O bond distances (1.61 Å) and the Si-O-Si (145°) and O-Si-O bond angles (109°). These restraints were gradually reduced and eventually completely relaxed. The position of OSDA in ZEO-2 was determined by combining simulated annealing and Rietveld refinement using high-resolution synchrotron diffraction data as described previously[38]. Shortly, the procedure can be described as follows: (1) refining the framework against the high-angle data only to extract a reliable scale factor, (2) retrieving the residual electron density inside the channel system corresponding to the position of OSDA from the difference electron density map using the whole dataset, as shown in Fig. S3a-S3c, (3) the OSDA was introduced into the channel system as a rigid-body to perform the simulated annealing. During the simulated annealing procedure, all the parameters were fixed except the translation and orientation of the OSDA. After obtaining the initial position of the OSDA, all the parameters were opened to refine one by one, such as peak shape, unit cell, instrument parameters, position of the framework atoms, and the torsion angles in OSDA molecule. After several cycles, the restraints were reduced from the refinement. With these processes, the OSDA was settled at the

intersection space of the ZEO-2 chains, which matched well with the residual electron density inside the channel system (Fig. S3). The detailed Rietveld refinement results for ZEO-2 and ZEO-3 are placed in Tab. S4.

Scanning transmission electron microscopy (STEM). High-resolution scanning transmission electron microscopy (STEM) was performed in an X-FEG FEI Titan low base equipped with a monochromator for the electron source and a CEOS spherical aberration corrector (Cs-corrected) for the electron probe assuring a 0.8 Å spatial resolution when operated at 300 kV as it was the present case. Sample preparation was done by deeply crushing the powder using mortar and pestle. To avoid any possible effect of the ethanol on ZEO-2, the crushed powder was directly deposited on the holey carbon Cu microgrid in dry conditions. ZEO-3 was prepared in a similar way but the crushed powder was dispersed in ethanol and few drops of the suspension were deposited onto holey carbon Cu grids. Due to the particular morphology of ZEO-3, the powder was embebed into a resin and ultramicrotomed to facilitate tilting the crystal along [001] zone axis. For imaging, annular bright field and annular dark field detectors (ABF and ADF) were used simultaneously. ABF data was employed for ZEO-2 to visualize the presence of the OSDA, while ADF was used for ZEO-3.

Multi-slice STEM simulations. To simulate the Cs-corrected STEM data we used the QSTEM program (www.qstem.org). The correspondent supercells were created for the distinct materials and orientations. The parameters used were: Cs = 0 mm, Uacc = 300 kV, an inner collection angle of 25 mrad for the ADF data and 5 to 25 mrad for the ABF; the half-convergence angle used was 15 mrad.

Framework energy minimization. The framework energy of ZEO-3 and sigma-**BEA** were calculated after energy minimization by the General Utility Lattice Program (GULP, gulp-6.0 [39,40]) using the polarizable Sanders-Leslie-Catlow (SLC) interatomic potential, with modified oxygen shell charge. The potential parameters are referred to previous report [41].

Dyes Adsorption. Similar to the previous protocols[6], the dyes adsorption of Nile Blue (NB, *i.e.* [9-(diethylamino)benzo[a]phenoxazin-5-ylidene]azanium chloride, $C_{20}H_{20}ClN_3O$) were performed on

two pure silica zeolites ZEO-3 and Beta. The ultraviolet and visible spectra of several standard NB solution (concentration from 1×10^{-4} to 2×10^{-6} mol/L) were collected on a UV-2401 PC spectrophotometer. The Lambert-Beer equation for NB at $\lambda = 595$ nm within the previous concentration range is: Int (a.u.) = 24214.94305 * *c* (mol/L).

VOCs Adsorption. In order to determine the adsorption equilibrium, static vapor-phase adsorption was performed using BELSORP-MAX. Each sample was degassed at 300 ^{o}C for 3 h. The measurements were carried out at 30 ^{o}C to construct the vapor adsorption isotherms. Breakthrough measurements were performed to study the dynamic adsorption behaviour in a fixed-bed reactor (6 mm i.d.). A gaseous mixture of C_7H_8 (about 800 ppm) and water vapor (relative humidity = 80%, when used) in a N_2 stream at a mass flow of 100 mL min^{-1} was fed into the reactor at a temperature of 30 ^{o}C. A mixture of 0.1 g adsorbent and 0.3 g quartz sand was packed in the bed. Prior to all adsorption measurements, samples were pretreated at 300 ^{o}C for 3 h. The concentrations of C_7H_8 was analysed online by a gas chromatograph (Kefen, GC-9160, SE-54 capillary column) with a flame ionization detector. To confirm the measurement of dynamic adsorption, temperature-programmed desorption (TPD) measurements were carried out after the breakthrough measurements. Once the samples were saturated by the VOC flow, the feed gas was changed to pure nitrogen to purge for 0.5 h, followed by temperature ramping to 400 °C at a linear rate of 2 °C min^{-1}. The product was monitored by the same GC instrument.

Data availability

The datasets generated during and/or analysed during the current study are available from the corresponding authors on reasonable request. Crystallographic parameters for the structure of ZEO-2 and ZEO-3 refined against SPXRD and cRED data are archived at the Cambridge Crystallographic Data Center (www.ccdc.cam.ac.uk/) under reference Nos. CCDC 2125815-2125816 (SPXRD data) and CCDC 2125677-2125678 (cRED data).

Methods references

32 Smeets, S., Wang, B. & Hogenbirk, E. instamatic-dev/instamatic: 1.7.0. (2021). https://doi.org/10.5281/zenodo.5175957.

33 Kabsch, W. Integration, scaling, space-group assignment and post-refinement. *Acta. Cryst. Sect. D* **66**, 133-144 (2010). doi:10.1107/S0907444909047374.

34 Wan, W., Sun, J., Su, J., Hovmoller, S. & Zou, X. Three-dimensional rotation electron diffraction: software RED for automated data collection and data processing. *J. Appl. Cryst*. **46**, 1863-1873 (2013). doi:10.1107/S0021889813027714.

35 Sheldrick, G. M. Phase Annealing in SHELX-90: Direct Methods for Larger Structures. *Acta Cryst. A* **46**, 467-473 (1990). doi: 10.1107/S0108767390000277.

36 Dolomanov, O. V., Bourhis, L. J., Gildea, R. J., Howard, J. A. K. & Puschmann, H. OLEX2: a complete structure solution, refinement and analysis program. *J. Appl. Cryst*. **42**, 339-341 (2009). doi.org/10.1107/S0021889808042726

37 Coelho, A. A. TOPAS and TOPAS-Academic: an optimization program integrating computer algebra and crystallographic objects written in C++. *J. Appl. Cryst*. **51**, 210-218 (2018). doi: 10.1107/S1600576718000183.

38 Smeets, S., McCusker, L. B., Baerlocher, C., Elomari, S., Xie, D. & Zones, S. I. Locating Organic Guests in Inorganic Host Materials from X-ray Powder Diffraction Data. *J. Am. Chem. Soc*. **138**, 7099-7106 (2016). doi:10.1021/jacs.6b02953.

39 Gale, J. D. & Rohl, A. L. The General Utility Lattice Program (GULP), *Mol. Simul*. **29**, 291-341 (2003). doi: 10.1080/0892702031000104887.

40 Gale, J. D. Analytical Free Energy Minimization of Silica Polymorphs, *J. Phys. Chem. B* **102**, 5423-5431 (1998). doi: 10.1021/jp980396p.

41 Schroder, K.-P., Sauer, J., Leslie, M., Catlow, C. R. A. & Thomas, J. M. *Chem. Phys. Lett*. *188*, 320-325 (1992). doi: 10.1016/0009-2614(92)90030-Q.

Acknowledgements. Financial support from the National Natural Science Foundation of China (grant numbers: 21601004, 21621001, 21776312, 22078364), the National Key Research and Development Program of China (Grant 2021YFA 1501202), the 111 project (B17020), the Natural Science Foundation of the Higher Education Institutions of Anhui Province, China (grant numbers: KJ2020A0585), and the Spanish Ministry of Science Innovation (PID2019-105479RB-I00 project, MCIN/AEI/10.13039/501100011033, and RYC2018-024561-I, Spain) is gratefully acknowledged. The cRED data were collected at the Electron Microscopy Center (EMC), Department of Materials and Environmental Chemistry (MMK) in Stockholm University with the support of the Knut and Alice Wallenberg Foundation (KAW, 2012-0112) through the 3DEM-NATUR project. Use of the Advanced Photon Source at Argonne National Laboratory was supported by the U. S. Department of Energy, Office of Science, Office of Basic Energy Sciences, under Contract No. DE-AC02-06CH11357. Additional funding from the European Union's Horizon 2020 research and innovation programme under grant agreement No 823717 - ESTEEM3 and the regional government of Aragon (DGA E13_20R) is also acknowledged. We thank Dr. Carlos Márquez (ICP-CSIC) for the FT-IR measurements, M. J. de la Mata (SIdI-UAM) for her expedited help in collecting MAS NMR spectra, and Dr. Agnieszka Ziolkowska (Umeå University) for her help in TEM sample preparation by ultramicrotomy.

Author contribution. F.-J.C. conceived the project. J.L., M.A.C., F.-J.C., and J.Y. supervised this work. Z.R.G., Q.-F.L., C.L. (Liu), F.G., S.Z., and F.-J.C. performed the synthesis work. J.L. solved the structure and performed Rietveld refinement and framework energy calculations. Z.R.G.

analysed the topology. J.L., Z.R.G., C.L. (Liu), C.L. (Lin), W.F., S.L., X.C., and M.A.C. carried out the physicochemical characterization. H.D. worked on the VOCs application. A.M. performed the HRSTEM tests. M.A.C. prepared the initial draft. J.L., W.F., M.A.C., F.-J.C., and J.Y. organized the work and the draft. All the authors discussed the results and revised the manuscript.

Competing interests. J.L., Q.-F.L., Z.R.G., C.L., and F.-J.C. have filed a patent on zeolites ZEO-2 and ZEO-3. J.L., Z.R.G., and C.L. are affiliated with the company holding the rights on that patent.

Additional information

Supplementary Information is available for this paper.

Correspondence and requests for materials should be addressed to J.L., M.A.C., F.-J.C or J.Y.

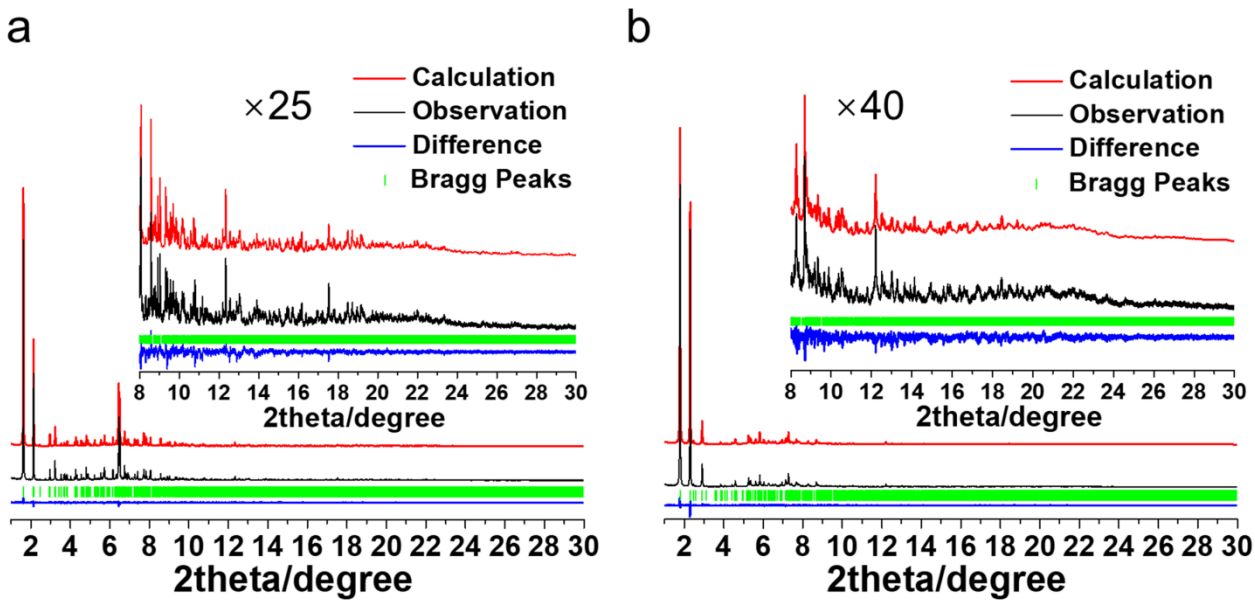

Extended Data Fig. 1 | Rietveld refinement plots of (a) ZEO-2 and (b) ZEO-3.

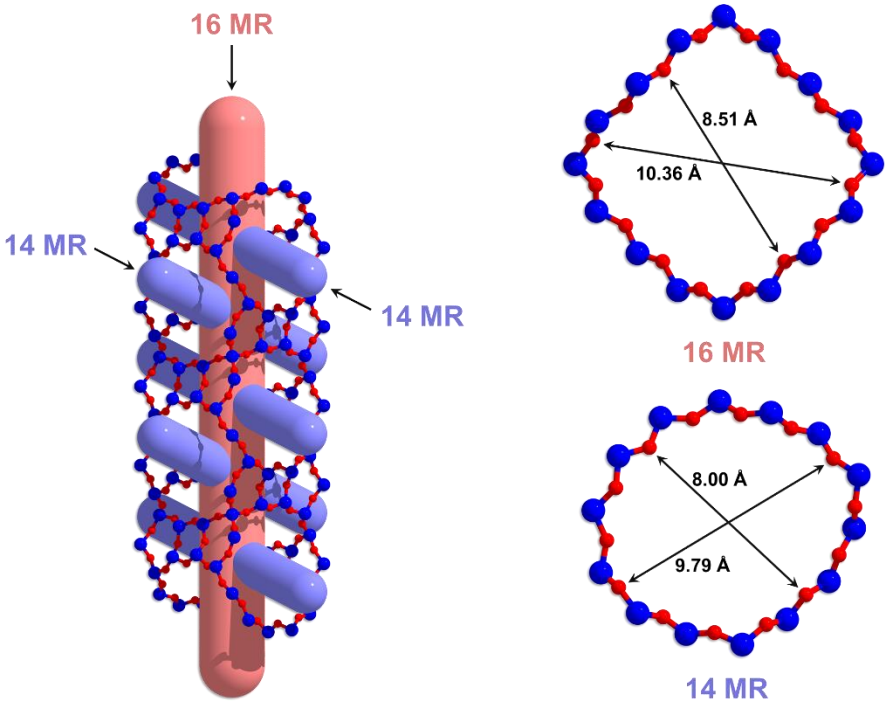

Extended Data Fig. 2 | 3D extra-large pore system (left) and the crystallographic pore size of ZEO-3 (right). The van der Waals radius of O (2×1.35 Å) has been subtracted.

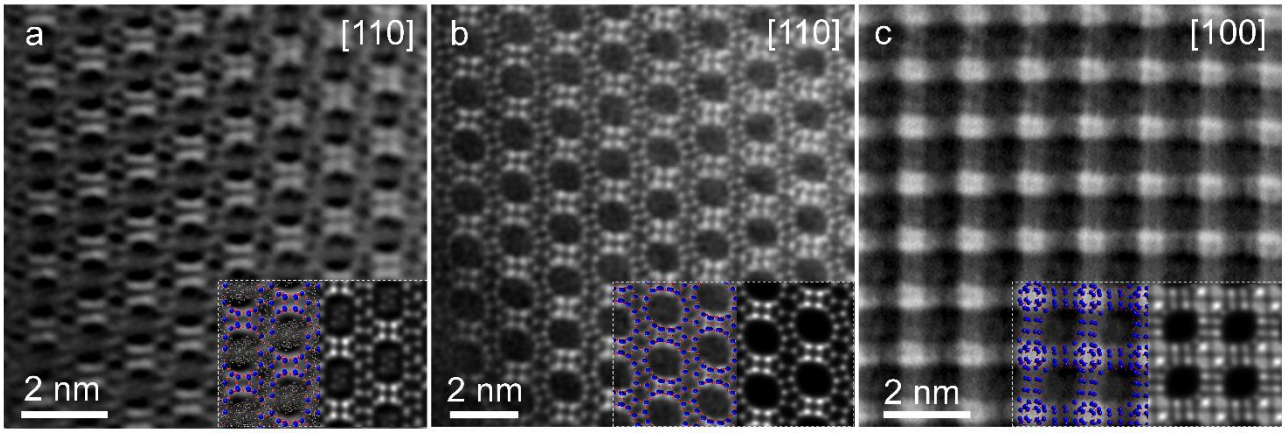

Extended Data Fig. 3 | Cs-corrected STEM visualization of the 1D silicate chain ZEO-2 along [110] projection (a), and the 3D extra-large pores of ZEO-3 along the [110] (14MR, b) and [001] (16MR, c) projections. The visualization along [001] suffers from a larger thickness (since this is the long needle direction) and the existence in the structure of atoms at different *z* levels that are displaced from one another along *x* and *y*. Along the [110] projection, the OSDA in the void between the silicate chain of ZEO-2 and the extra-large 14MRs in ZEO-3, as well as all other rings (4Rs, 5Rs and 6Rs) are clearly visible. To facilitate image interpretation, the schematic models (Si atoms in blue and O atoms in red) have been superimposed and the simulated STEM images are also included in the right bottom inset.

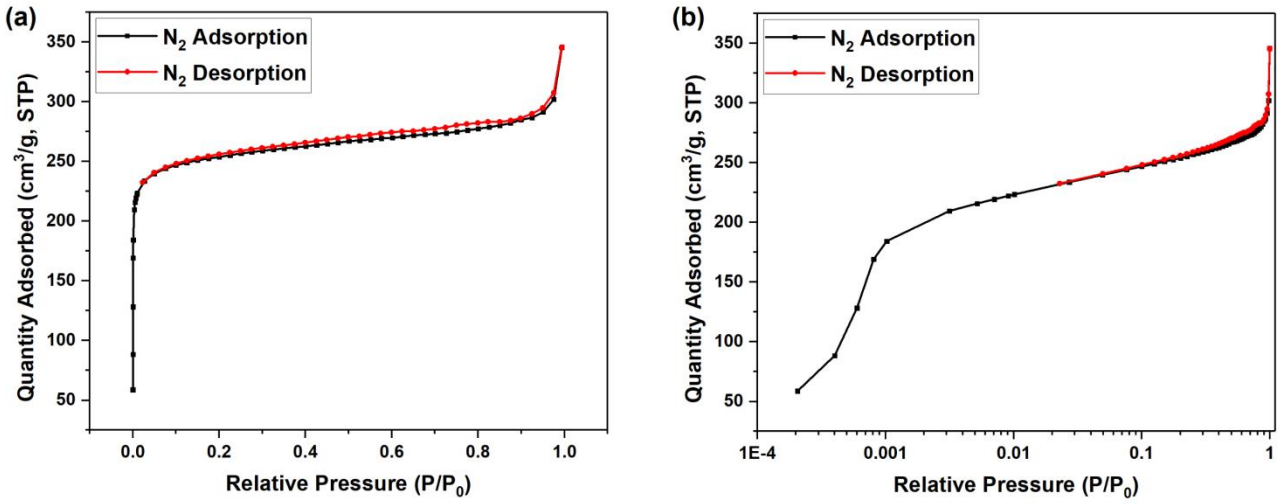

Extended Data Fig. 4 | N_2 adsorption/desorption isotherm of P-free ZEO-3 at 77 K, with x-axis in (a) linear and (b) logarithmic scale, respectively.

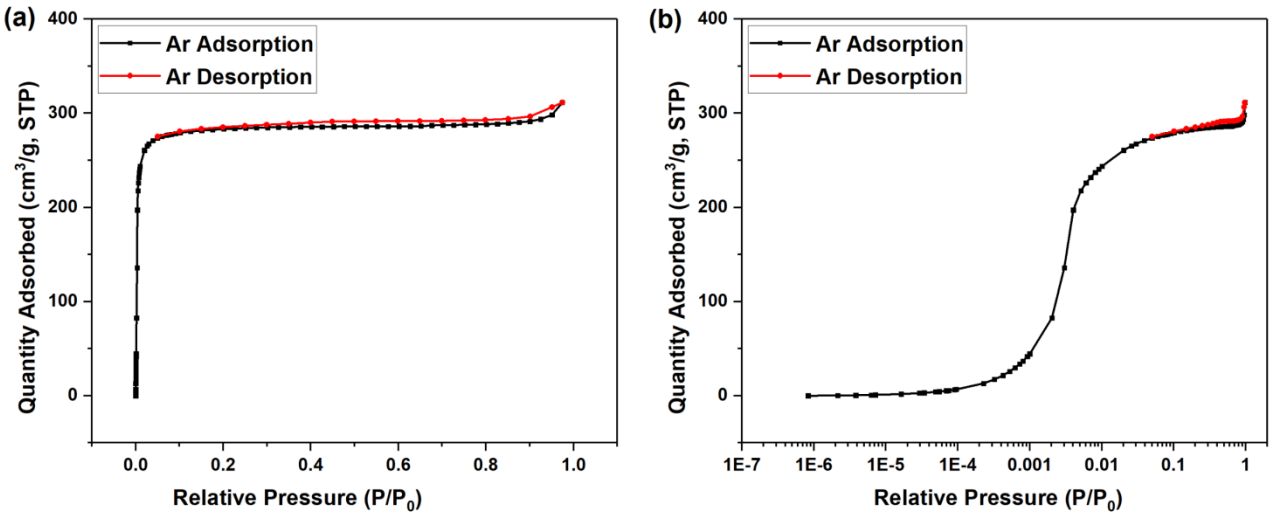

Extended Data Fig. 5 | Ar adsorption/desorption isotherm of P-free ZEO-3 at 87 K, with x-axis in (a) linear and (b) logarithmic scale, respectively.

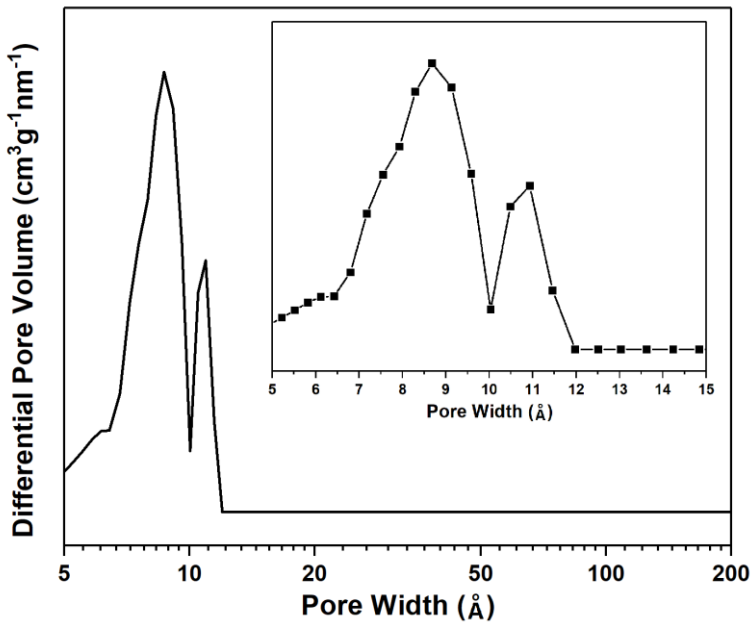

Extended Data Fig. 6 | Pore size distribution of P-free ZEO-3 from Ar adsorption isotherm at 87 K, where the main figure shows the logarithmic scale of x-axis and the inserted figure shows the linear scale.

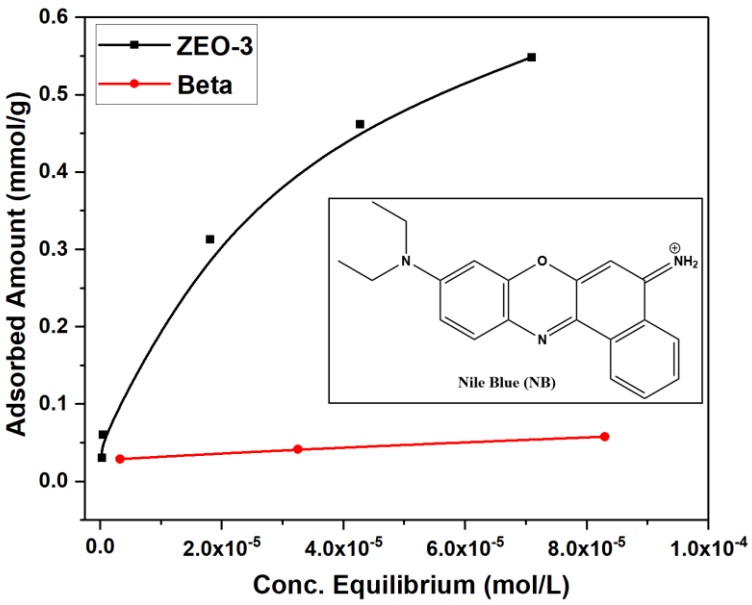

Extended Data Fig. 7 | Nile Blue adsorption isotherms on the pure silica 16×14×14 MR ZEO-3 (black curve) and 12×12×12 MR Beta (red curve) zeolites, with the inserted figure of molecular structure of Nile Blue. These data show ZEO-3 has potential for the removal of large organic pollutants.

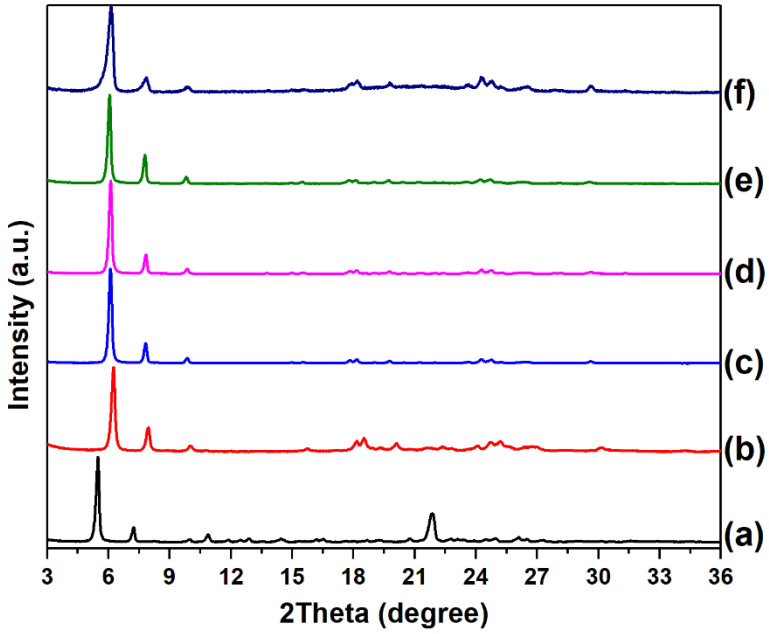

Extended Data Fig. 8 | PXRD patterns of ZEO-2 and ZEO-3: (**a**) as-synthesized ZEO-2, (**b**) calcined ZEO-3 in air at 600 ^{o}C for 6 hours, (**c**) P-free ZEO-3 from H_2 reduction at 600 ^{o}C, (**d**) 800 ^{o}C calcined in air (with one-hour plateau) on the P-free ZEO-3, (**e**) 1100 ^{o}C calcined in air (with one-hour plateau) and (**f**) after hydrothermal treatment at 760 ^{o}C with 10% H_2O vapor for 3 hours on the P-free ZEO-3.